Molecular BioSystems

Accepted Manuscript

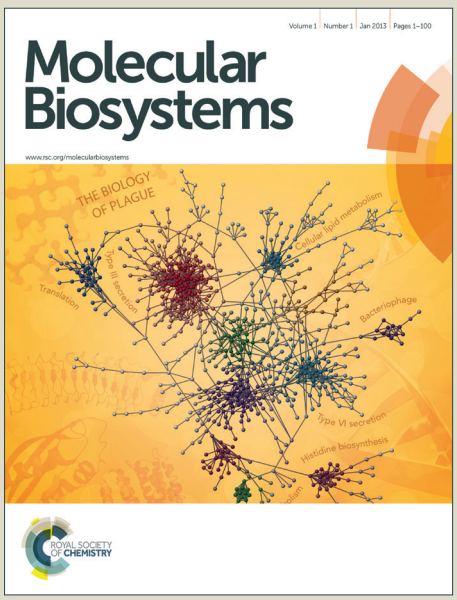

ROYAL SOCIETY OF CHEMISTRY

www.rsc.org/molecularbiosystems

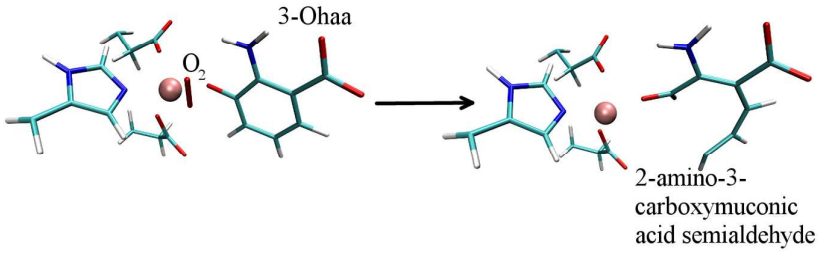

The 3-Ohaa oxidation mechanism catalysed by 3HAO and influence of mutations on the 3HAO structure and dynamics are presented.

Journal Name

RSCPublishing

ARTICLE

Human 3- hydroxyanthranilate 3,4-dioxygenase (3HAO) dynamics and reaction, a multilevel computational study

Cite this: DOI: 10.1039/xoxxoooooox

Received ooth January 2012,
Accepted ooth January 2012

DOI: 10.1039/xoxxoooooox

www.rsc.org/

H. Brkić,[a] B. Kovačević[b] and S. Tomić[b] ,

3-hydroxyanthranilate 3,4-dioxygenase (3HAO) is a non-heme iron dependent enzyme. It catalyses the cleavage of the benzene ring of 3-hydroxyanthranilic acid (3-Ohaa), an intermediate in the kynurenine pathway and because of that represents a potential target in treating numerous disorders related to the concentration of quinolinic acid (QUIN), the kynurenine pathway product, in tissues. Stability and behaviour of the enzyme in nearly physiological conditions, studied by the empirical molecular modelling methods enabled us to determine influence of several, for the enzyme activity relevant, point mutations (Arg43Ala, Arg95Ala and Glu105Ala) on the protein structure, particularly on the active site architecture and the metal ion environment, as well as on the substrate, 3-Ohaa, binding. Besides, the water population of the active site, and the protein flexibility as well as the amino acid residues interaction networks relevant for the enzyme activity were determined for the 3-Ohaa complexes with the native and mutated enzyme variants. Finally, using the hybrid quantum-mechanics/molecular-mechanics (QM/MM) calculations the 3HAO catalysed 3-Ohaa oxidation into 2-amino-3-carboxymuconic acid semialdehyde was elucidated.

Introduction

3-hydroxyanthranilic acid dioxygenase (3HAO; 3-hydroxy-anthranilate 3,4-dioxygenase, EC 1.13.11.6) is an enzyme directly involved in the quinolinic acid (QUIN) synthesis.
It is a monomeric cytosolic protein (consisting of 286 amino acid residues)[1] belonging to the family of intramolecular dioxygenases containing non-hem ferrous iron (Fe^{2+}). Similarly to the other dioxygenases, it catalyses incorporation of the atmospheric oxygen into the substrate, wherein the iron ion activates the molecular oxygen and lowers the reaction barrier. 3HAO catalyses the cleavage of the benzene ring of 3-hydroxyanthranilic acid (3-Ohaa), an intermediate in the kynurenine pathway. The product of the interaction is an unstable intermediate, 2-amino-3-carboxymuconic acid semialdehyde, which can spontaneously rearrange to QUIN. 3HAO is widely distributed in peripheral organs, such as liver and kidney, and its role is indicated in several diseases related to the level of QUIN in the tissue[2]. In low amounts it is also present in the central nervous system[3].
Schwarcz et al[4] reported an increase of 3HAO in cerebral tissue in Huntington's disease patients. In a rat model of epilepsy, 3HAO-positive gill cells have been reported to become highly hypertrophied in the brain areas where neurodegeneration occurred[5]. Besides, the kynurenine pathway disorder is indicated in some infective disease (*e. g.* HIV), as well as in autoimmune (multiple scleroses and rheumatoid arthritis), cardiovascular and malignant diseases[6]. Apparently, understanding the behaviour of 3HAO in cells and, in context of this, elucidation of its catalytic mechanism is important for understanding a number of physiological processes in which it was implicated.
Besides the human 3HAO structure (PDB_code 2QNK[7]) the crystallographic structures of several other orthologs, e.g of 3HAO from bacteria (Saccharomyces cerevisiae and Ralstonia metallidurans) and of 3HAO from the bovine kidney, are available as well. In contrast to bacterial, the bovine and human proteins are monomeric bicupins lacking the rubredoxin-like centre (at C terminus), with only the N-terminal cupin domain containing an active site. However, the all 3HAO proteins characterized until now depend on Fe^{2+} for activity and the active-site residues that are considered to be relevant for the catalytic reaction appear to be fully conserved among the known orthologues.[8] According to the EPR study[9] exposure of native 3HAO to oxygen results with the metal ion oxidation (Fe^{2+} to Fe^{3+} transition) and enzyme autoinactivation. However, in the presence of substrate the iron ion activates O_2 and the reaction (incorporation of O_2 into the substrate) proceeds. Our molecular modelling study revealed influences of point mutations to the protein structure and flexibility and enabled us to rationalize the experimentally determined decrease of the enzyme activity in the case of polar amino acid

residue mutants (Arg43Ala, Arg95Ala and Glu105Ala). Further on, using the combined QM/MM approach we were able to model the enzymatic reaction, namely the oxidative transformation of hydroxyanthranilic acid to 2-amino-3-carboxymuconic acid semialdehyde catalysed by 3HAO (Figure 1). To the best of our knowledge this is the first molecular modelling study performed for a 3HAO orthologue.

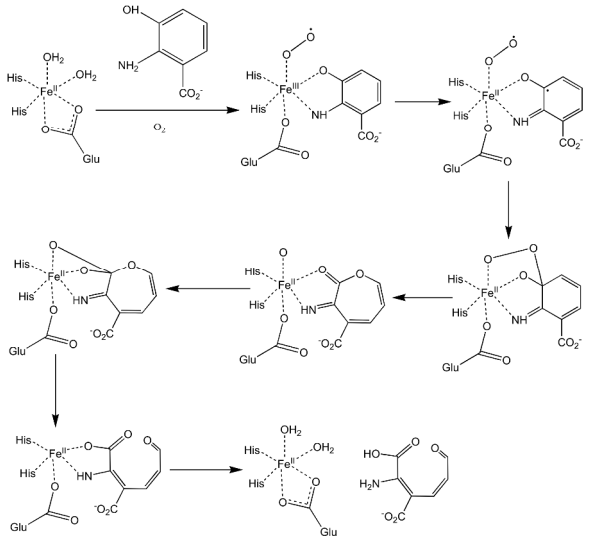

Figure 1. Schematic representation of the reaction mechanism, proposed by *Zhang et al*. [10] for oxidation 3-Ohaa into 2-amino-3-carboxymuconic acid semialdehyde catalysed by 3HAO.

Materials and methods

System preparation for MD simulations. As the starting point for our molecular modelling study we used the 3D structure of human 3HAO, determined by x-ray diffraction crystallography (PDB_code 2QNK, resolution 1.60 Å)[7]. The nickel present in this structure was replaced by iron, the metal needed for the catalysis. The phosphate ions were removed and the unnatural amino acid residue, selenomethionine (used to stabilize the crystal structure) was replaced by methionine. Non-polar hydrogen atoms were added by *tleap*, the AMBERTools12 (http://ambermd.org/)[11] module and polar hydrogen atoms were added manually to optimize the hydrogen bonds network in the protein and to arrange the proper metal ion environment. The substrate, 3-hydroxyanthranilic acid (3-Ohaa) was built by the programme VMD[12] (http://www.ks.uiuc.edu/Research/vmd/). Parameterization was performed by the AMBERTools12 modules *antechamber* and *tleap* using GAFF[13] and ff12SB[14] force fields to parameterize the substrate and the protein, respectively. Bonding parameters for Fe^{2+} were taken from our previous work[15], while the Fe^{2+}, O_2, and the substrate charges were derived using electrostatic potential (ESP) with quantum mechanical (QM) B3LYP/6-31G(d,p)[16] calculations on the model system consisting of 94 atoms (see Supplemental Figure S1) by program Gaussian09[17]. Because of the iron ion vicinity and the substrate stabilization within the enzyme active site by arginines, the pKa value of the hydroxyl group is probably very low. To test this hypothesis we calculated the proton affinity (PA) of the substrate dianion in a free form and bound in the active site. Utilizing the aforementioned theoretical model we found that the PA for protonation of substrate dianion at O^- equals 320.7 kcal mol^{-1} when substrate is bound in the active site (calculated on model system). The PA of free (not in the active site) substrate dianion calculated at CPCM/ B3LYP/6-31G(d,p) with ε = 4 is 339.3 kcal mol^{-1}, a value comparable to the PA of tyrosine in the hydrophobic environment[18]. It appears that the substrate binding into the active site significantly decreases the hydroxyl anion PA, mainly due to the strong Fe-O^- interaction. The decrease in PA of 18.6 kcal/mol corresponds roughly to the pKa decrease of 13.7 units. A similar decrease in pKa value (18 units) was reported recently for cysteine residue upon binding of the Cd^{2+} cation[19]. Consequently, we propose that the substrate is present in the dianion form in the enzyme active site.

Based on the sequence alignment (BLAST[20]) the mutants of the human orthologue equivalent to the bacterial 3HAO mutants Arg47Ala, Arg99Ala and Glu110Ala (for which the kinetic measurements had been performed[10]) were identified to be Arg43Ala, Arg95Ala and Glu105Ala, respectively.

The substrate docking was performed with the program Autodock (Autodock vina 1.1.2.)[21], but taking into account the ligand orientation in the active site of the bacterial enzyme (PDB_code 1YFY). Despite the quite low sequence identity between the two orthologues, bacterial and human, (37%, according to blast2seq) the binding site architecture is entirely preserved. The ligand free 3HAO as well as its complexes with 3-Ohaa were solvated in an octahedron box filled with TIP3P water molecules[22] ensuring 8 Å thick buffer of water molecules around the protein. Na^+ ions, added to neutralize the system, were placed in vicinity of the charged amino-acid residues at the protein surface.

Molecular dynamics simulations. The resulting systems, consisting of ~39 000 atoms, were simulated using periodic boundary conditions[23]. The electrostatic interactions were calculated using the particle-mesh Ewald method[24]. Both, minimization and molecular dynamics (MD) simulation were performed by *pmemd* module running at GPU[25, 26]. Before MD simulations, the protein geometry was optimized in four cycles (10 000 steps each) with different constraints. In the first cycle, waters and substrate molecule were relaxed, while the protein and the iron ion were constrained using a harmonic potential with a very high force constant of 500 kcal/(molÅ^2). In the second and third cycle, the constraint imposed to the iron ion was reduced to 50 and 32 kcal/(molÅ^2), respectively while the protein backbone was constrained with 50 and 10 kcal/(molÅ^2), respectively. In the final cycle the protein backbone was constrained with 5 and the iron ion with 12 kcal/(molÅ^2). The energy minimization procedure was the same in all four cycles: After 5000 steps of steepest descent 5000 steps of conjugate gradient optimization was applied. The minimized system was heated from 0 to 300 K during 10 ps using canonical ensemble (NVT). Followed seven equilibration stages, 10 ps each, during which the water density was adjusted and the initial constraints on the protein and the metal ion were gradually reduced. The equilibrated system was then subjected to 100 ns of the productive MD simulations using the NPT ensemble. The constant temperature (300 K) and pressure (1 atm) were ensured using Langevin dynamics[27], with the collision frequency of 1 ps^{-1}, and the Berendsen barostat[28], respectively. The time step was 2 fs (SHAKE[29] algorithm was used to restrain motion of hydrogens). The identical procedure was applied for all systems, the ligand free enzyme and the complexes (WT, Arg43Ala, Arg95Ala Glu105Ala) with 3-Ohaa. In order to equilibrate substrate in the orientations which we considered as the most appropriate for modelling the oxidative transformation of 3-Ohaa, the bonding parameters between the iron ion and the substrate were gradually reduced during the simulations (see

Supplemental Table S1). It is important to notice that during the last 30 ns of simulations the interactions of the iron ion with environment were modelled using exclusively nonbonding parameters (*i.e.* parameters required to model van der Waals and electrostatic interactions).

MM-PBSA free energy calculations. In order to determine the relative substrate binding affinities the Molecular Mechanics Poisson−Boltzmann Surface Area (MM−PBSA) calculations[30], as implemented in the AMBER10 suit of programs, have been performed on the 2-ns long final parts of the MD simulation trajectories. The concentration of the singly charged counterions was 0.1 M. The polar component of solvation enthalpy was calculated using the Poisson−Boltzmann method, and the nonpolar component was determined by $\Delta_{sol}H_{nonpolar}=\gamma SASA+\beta$, where the solvent accessible surface area (SASA) was calculated with the MolSurf program[31]. The surface tension γ and the offset β were set to the standard values of 0.0072 kcal/mol Å^2 and 0.0, respectively. The calculations were accomplished for the enzyme immersed into the solvent utilizing the solute dielectric constant of 4.0.
The substrate binding site in 3HAO is water exposed and the water molecules take an active role in the substrate stabilization. Because of that the water molecules present within 3 Å of the substrate during the last 20 ns of MD simulations were considered as a part of enzyme in the MM_PBSA calculations.
Since the ligand binding is accompanied with expel of the water molecules from the enzyme active site, we determined the substrate affinity as a difference between the water and the ligand binding enthalpies. For this purpose water molecules coordinating the metal ion during at least 30% of the simulation time were considered as 'bound'.

Modelling of the 3HAO catalysed reaction – QM and QM/MM calculations. In order to determine the reaction mechanism for oxidative transformation of 3-hydroxyanthranilic acid we used the quantum-mechanical (QM) and the combined quantum-mechanical/molecular-mechanics (QM/MM) approaches. Calculations were performed by the program package Gaussian09[17]. QM calculations were performed using the model system consisting of the metal ion, substrate and the amino acid residues His91 (ε-protonated), His47 (δ-protonated), Glu49, Glu53 and Arg43 (Figure 2). The amino acid residues were represented by their side chains starting from C_β atom, and in the case of Arg starting from C_γ atom, with H atom added to the tetrahedral C_β (C_γ) terminal carbons. The model system had altogether 76 atoms. Calculations were performed using the conductor-like polarizable continuum model (CPCM)[32] to model the electrostatic component (reaction field) of the protein, i. e. an environment with the dielectric constant set to 4. The geometry optimization was performed using the DFT approach at B3LYP/6-31G(d,p)[16] level for all atoms except iron, which was described using the SDD[33] basis set. The net charge of the model system was -1e (Fe^{2+}, $Glu49^-$, $Glu53^-$, $Arg43^+$, 3-$Ohaa^{2-}$).
The initial system used in the QM/MM calculations was obtained as a result of the MD simulations. Since the MD simulations revealed two stable substrate binding modes the binding free energies were calculated (using MM_PBSA method), and the mode with predicted higher affinity was utilized in further QM/MM calculations to model the enzyme catalysed reaction. In order to make the simulated system appropriate for this type of calculations, the number of water molecules was reduced using the TAO package[34] (surface residues were listed and only water molecules within 3 Å of them were kept). Finally, the initial system consisted of 10746 atoms with 65 of them treated quantum-mechanically. The "QM region" comprised the metal ion (Fe^{2+}), the substrate (3-$Ohaa^{2-}$) and the amino acid residues His91 (ε-protonated), His47 (δ-protonated), $Glu49^-$, $Glu53^-$ and $Arg43^+$ (Figure 2). The MM calculations were performed using AMBER force field (parm96[14] with its current updates), while the "QM region" was modelled using the B3LYP/6-31G calculations.

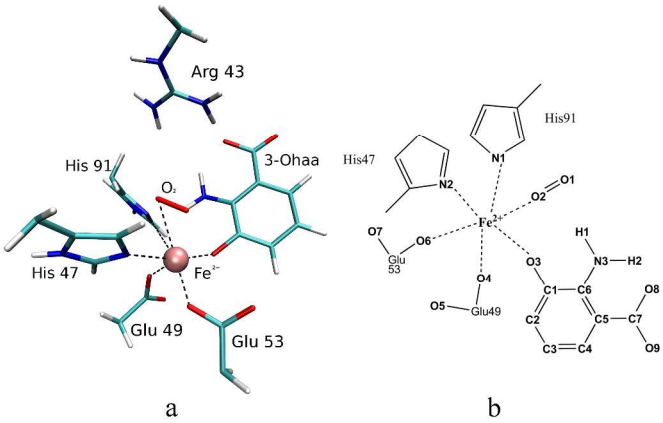

Figure 2. The "QM region" of the system used to study the 3HAO catalysed reaction: **a)** real system, **b)** schematic representation, the atoms that actively participate in the reaction are labelled.

The QM/MM geometry optimization was performed for the "QM region" and all amino acid residues within 8 Å of the "QM region". In order to model the oxidative transformation of 3-Ohaa we defined six one dimensional reaction coordinates: a) O1 – C1, b) O1 – O2, c) O1 – C2, d) C1 – C2, e) O2 – C1, and f) C1 – O1 distances (see Figure 2b. for atom names). Energies of the stationary points (transition states and minima) were corrected by the single point calculations using the larger basis sets 6-311+G(2d,p) and TZVP[35, 36]. The transition states and minima, initially determined as the "highest" and the "lowest" points, respectively on the potential energy surface along the reaction coordinates, were verified using the frequency analysis. The reaction profile was determined using the mechanical embedding scheme. Subsequently, in order to include the polarizing effect of the enzymatic environment on the QM region, the electrostatic embedding[37] was applied.

Results and discussion

In order to investigate the influence of the ligand binding and of the point mutations on the structural and dynamical properties of human 3HAO, as well as to obtain reliable starting structures for modelling the enzymatic reaction, the MD simulations have been performed for a series of the enzyme variants (native and mutated) and their complexes with substrate (3-Ohaa).

MD simulations and the structure analysis of the human 3HAO variants

Overall protein structure. Influence of the substrate binding as well as of the point mutation to the overall protein structure was analysed. For this purpose, besides for the whole protein, the RMSD values for the protein regions defined according to their sequence position, and the secondary structure, were considered (Figure 3). RMSD for the each region, with respect to the initial

structure, was monitored during the last 20 ns of, in total, 100 ns of MD simulation. The substrate binding has not influenced significantly the protein conformation, i. e. the mutual position of beta barrels and the adjacent alpha helices (Supplemental Figure S2) have not changed upon ligand binding, only the solvent exposed loop comprised of the amino acid residues 166 to 180, as well as the protein C terminus (AAs 279-286) slightly reoriented. The point mutations also have not significantly influenced the protein secondary structure, nor its conformation (see Table 1 and Supplemental Figure S3). However, both the ligand binding and the point mutations significantly influenced the protein flexibility. The substrate binding resulted with reduction of the overall protein flexibility (Supp. Fig. S2) while the point mutations induced an increase of the protein flexibility especially of the C-terminal half of the protein, and the solvent exposed loop (166-180). The Arg95 to Ala mutation induced the most drastic changes.

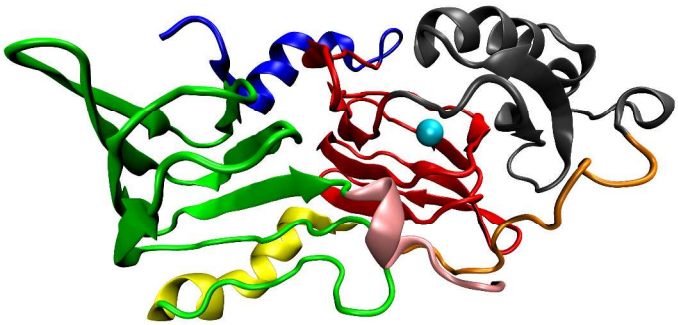

Figure 3. The protein secondary structure elements grouped according to vicinity of the amino acid residues in sequence (1-23 (blue), 24-107 (red), 108-165 (grey), 166-180 (orange), 181-197 (yellow), 198-278 (green) and 279-286 (pink)). The metal ion is displayed as the cyan ball.

Despite the increased flexibility of the mutants, the overall protein structure was quite stable in all simulated systems. Interestingly, the completely solvated C-terminus (amino acid residues 278-286) in the native (wild type) protein complex changed its orientation much more than in the mutant complexes during the simulations (Supplemental Figures S2 and S3).

The iron ion coordination sphere. The number of atoms that coordinate Fe^{2+} during MD simulations is given in Table 2. In the ligand free enzyme Fe^{2+} is mostly hexacoordinated (>66% of the simulation time, similar coordination has Ni^{2+} in the crystal structure), while in the complexes with 3-Ohaa number of coordinating atoms reduced to 5. The main reason is reduction of water population in the metal ion coordination sphere. Namely, upon ligand binding the number of water molecules in the first coordination sphere reduced from two (ligand free protein) to 0 (complexes) (see Table 3).
In all systems His47 and His91 coordinated the metal ion during the entire simulations (see Supplemental Figure S4). The same is true for Glu53 except in the case of Glu105Ala – 3-Ohaa complex where, after about 40 ns of MD simulations, Glu53 left the iron coordination sphere. In most complexes Glu49 entered the metal ion coordination sphere already during equilibration, however in the ligand free enzyme it was 6-7 Å from Fe^{2+} during the entire simulation. The most common metal ion coordinations, determined during the simulations of the ligand free protein and of its complex with 3-Ohaa, are shown in Figure 4.

Table 1. The percentage of secondary structure elements in the initial (experimentally determined) 3HAO structure and in the structure of the simulated variants.

The secondary structure	Initial structure	WT	Enzyme complexes with 3-Ohaa			
			WT	Arg43 Ala	Arg95 Ala	Glu105 Ala
	%	%	%	%	%	%
H	14.6	10.8	12.2	10.5	8.7	12.2
G	3.2	2.1	2.4	3.1	5.2	4.5
E	39.3	40.9	40.2	43.7	43.0	44.1
T	21.1	26.2	24.5	23.8	20.6	18.9
C	19.6	19.2	20.6	18.9	21.7	20.3

Table 2. Number of atoms that coordinate Fe^{2+} during the MD simulations. Percentage of the simulation time that each of the coordination type is present during the simulation is given.

Coordi-nation number	Ligand free enzyme	Enzyme complexes with 3-Ohaa			
		WT	Arg43 Ala	Arg95 Ala	Glu105 Ala
	%	%	%	%	%
4	0.3	1.6	0.9	0.5	2.1
5	32.9	89.7	93.9	95.7	76.3
6	66.7	8.7	5.2	3.8	21.6
7	0.1	0.0	0.0	0.0	0.0

Table 3. Number of water molecules that coordinate Fe^{2+} during the MD simulations (given in percentage of the simulation time).

# water mole-cules	Ligand free enzyme	Enzyme complexes with 3-Ohaa			
		WT	Arg43 Ala	Arg95 Ala	Glu105 Ala
	%	%	%	%	%
0	0.1	85.2	94.4	87.4	26.1
1	32.1	14.8	5.6	12.6	56.4
2	67.7	0.0	0.0	0.0	17.5
3	0.1	0.0	0.0	0.0	0.1

In both systems histidines (His47 and His91) and Glu53 are constituents of the Fe^{2+} first coordination sphere. However, in the ligand free protein Glu53 coordinates the metal ion bidentantely and in the complexes with 3-Ohaa monodentantely. Instead, in the complexes, the Glu49 carboxyl oxygen entered the first metal ion coordination sphere (Figure 4b), and the water molecules are replaced by the substrate. In the all complexes 3-Ohaa constantly coordinated Fe^{2+} during the 100 ns long MD simulation (and this interaction is only slightly stronger in the complex with the WT enzyme; 1.78 Å average distance in WT, and 1.8 Å or higher in mutants).

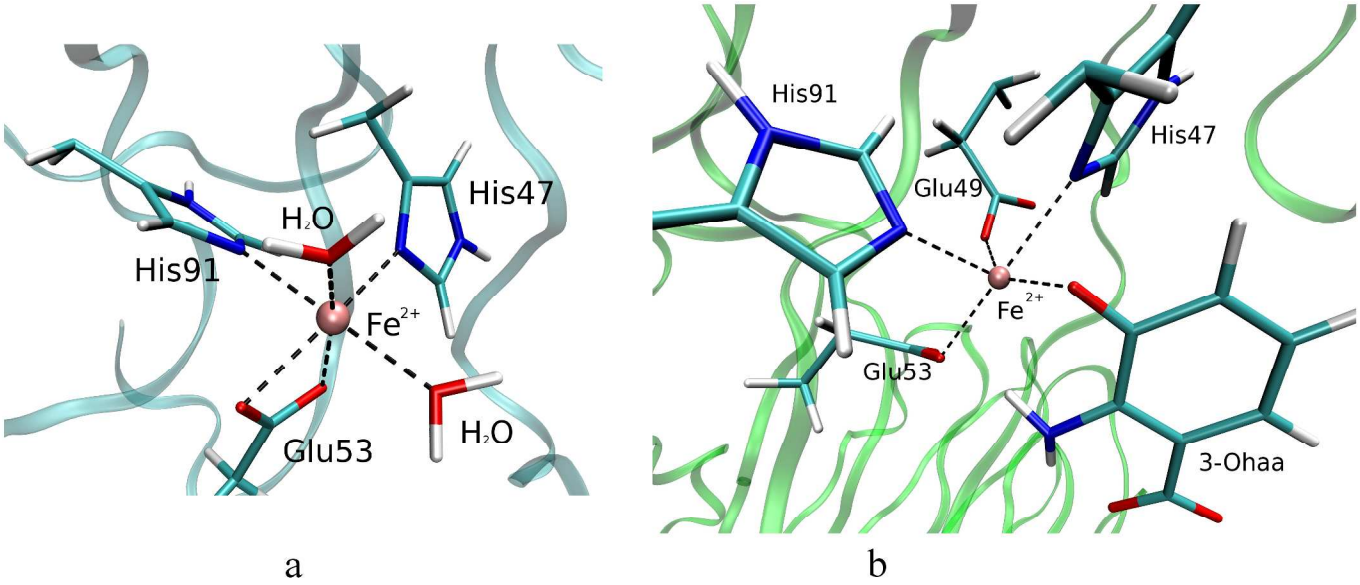

Figure 4. The first coordination sphere of Fe^{2+} in the native human 3HAO; **a)** ligand free, and **b)** in the complex with 3-Ohaa. An atom is considered as a metal ion ligand if it is within 2.5 Å of the metal centre (Fe^{2+}).

Our simulations showed that the substrate bound in the enzyme active site hinders water molecules to freely access the metal ion in the complexes. However, the Glu105 to Ala mutation increased the metal ion solvent accessibility resulting with larger population of the hexacoordinated Fe^{2+} in the Glu105Ala with respect to the other complexes (Table 3). The Glu53 position is, besides its attractive interaction with Fe^{2+}, determined also by the Glu53 – Glu105 water mediated interaction. By the Glu105 to Ala mutation this interaction is lost and as a consequence the Glu53 side chain reoriented toward the newly formed empty space in the direction of Ala105 and left the metal ion coordination making it more solvent accessible (see Supplemental Figures S4 and S5). So, although, according to the MM-PBSA binding free energy calculations and the experimentally determined Michaelis constant, K_m (Table 4 and Supplemental Table S2, respectively) the substrate binds with higher affinity to the Glu105Ala mutant than to the wild type protein, its chemical transformation is less efficient because the water molecules in the iron ion coordination sphere hinder binding of the oxygen molecule.

Arg43 and Arg95 do not constitute the metal ion binding site and do not influence its coordination. They are H-bonded to Asp45 and Met62, respectively (Supplemental Figure S6) and constitute the positively charged patches at the edge of the substrate entering hatch (see Supplemental Figure S5). Their mutation to Ala resulted in a decrease of the enzyme activity by two orders of magnitude (see Supplemental Table S2). Both Arg43 and Arg95 take part in the substrate stabilization (see Figure 5, Supplemental Figure S5 and Supplemental Table S3). It should be noted that their interaction with the substrate is concerted. So, the interaction between Arg43 and substrate, strong in most of the analysed complexes, is negligible in the Arg95Ala mutant (see Supplemental Figure S6). In the Arg mutants substrate interactions with Leu137 and Gly138 are also weakened in comparison to the interactions in the complexes with the wild type enzyme and the Glu105Ala mutant; however, the interaction between the substrate and Glu53 is stronger in the complexes with Arg mutants (Supp. Table S3).

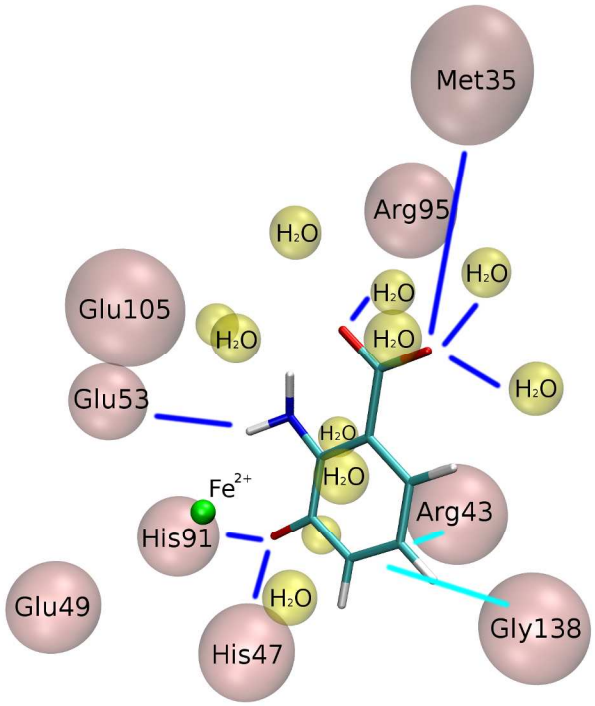

Figure 5. Schematic representations of the protein – substrate, 3-Ohaa, interactions and of the metal ion environment. Dark blue lines represent hydrogen bonds, while the cyan lines represent the electrostatic and van der Waals interactions.

Besides of the reduced substrate affinity of the Arg mutants with respect to the wild type protein and especially with respect to the Glu105Ala mutant (as could be also concluded from both, the measured K_m and the binding free energy calculations, Table 4 and Supplemental Table S2, respectively), a possible reason for the lower enzyme activity could be lower potency of Fe^{2+} to activate the oxygen molecule. Namely, the positively charged guanidino groups of Arg43, which is close to the metal center, probably take part in ferrous stabilization. By replacement of the charged Arg with the neutral Ala, the Fe^{2+} to Fe^{3+} transition could easier occur, and consequently, inactivate the enzyme[9]. Further on, according to the QM/MM calculations (see below), Arg43 is directly involved in stabilization of the

transition state. So, we could assume that in the Arg to Ala mutants this stabilization, and consequently the enzymatic activity, is reduced.

The relative binding affinities (the second row in Table 4) determined by MM_PBSA calculations have a similar trend as the experimentally determined K_m values (Glu110Ala has the lowest, followed WT, and the Arg mutants; see Supplemental Table S2). However, caution is needed when comparing Michaelis (K_m) and dissociation constants (K_d) since the previous, besides substrate affinity, incorporates effects of transition state stabilization and product release rates. Besides, the experimental values are for the bacterial and the calculated ones for the human ortholog.

Reaction mechanism catalysed by 3HAO (QM/MM) calculations

In order to check the reaction mechanism proposed by *Zhang et al.*[10] (Figure 1) we first performed the QM calculations for the model systems.

QM calculations The coupling of triplet O_2 with quintet Fe^{2+} gives rise to three possible spin states, the high-spin (HS) septet, intermediate spin (IS) quintet and low-spin (LS) triplet. Taking into account the results obtained by *Dong at al.*[38] who modelled the homoprotocatechuate 2,3-dioxygenase catalysed reaction, and the similarity between the iron coordination in the enzymes, as well as the spectroscopic results on 3HAO (and Dke1[39]), we assumed the quintet state as the most appropriate for our system. We also confirmed this premise with preliminary calculations.

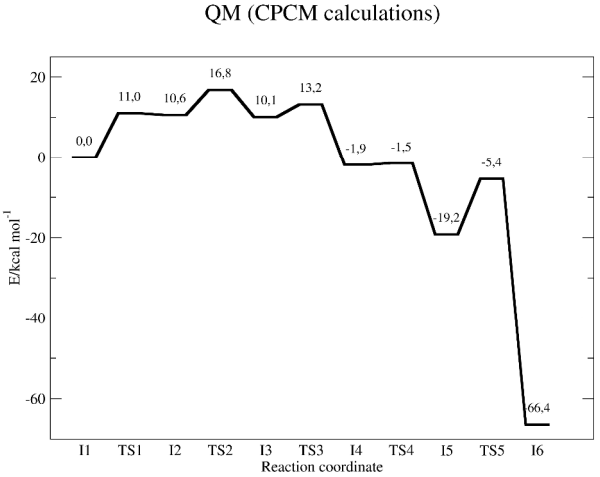

Figure 6. The energy profile for the reaction mechanism obtained for the model system by QM (B3LYP/6-31G(d,p)) calculations using the CPCM polarization (black line).

The reaction profile obtained using the CPCM polarization model is given in Figure 6, and reaction scheme is shown in Figure 7. TS2 (with the energy, relative to the initial state, of 16.8 kcal mol^{-1}) was determined as the transition state with highest energy. The nature of the stationary points was proven by the frequency analysis. The systems with reactant, product and intermediates (Is) do not have imaginary frequency, while the each transition state has exactly one imaginary frequency.

QM/MM calculations. In order to determine the influence of the enzyme environment on the course of the reaction (Figure 7), and eventually to obtain a more realistic reaction profile, we performed QM/MM calculations. The stationary points together with the reaction coordinate values and their relative energies (with the zero point vibrational energy included) are shown in Figure 8. The energy profiles determined using both, B3LYP/6-311+G(2d,p)//B3LYP/6-31G and B3LYP/TZVP//B3LYP/6-31G, level of theory (see Figure 9) are similar to the one determined on the model system.

Table 4. MM_PBSA energies calculated for the 3HAO-3-Ohaa complexes using the snapshots collected during the last 2 ns of MD simulations, the substrate affinities relative to the water affinities (the 1st column) and the relative affinities for 3-Ohaa binding to different variants (the last four columns).

[kcalmol^{-1}]	WT ΔG_{wat}	WT1 ΔG_{lig}	Arg43 Ala ΔG_{lig}	Arg95 Ala ΔG_{lig}	Glu105 Ala ΔG_{lig}
MM_PBSA energies	-1 ± 2	-275 ± 6	-270±6	-274±4	-286±7
The relative substrate affinities		**11**	**16**	**12**	**0**

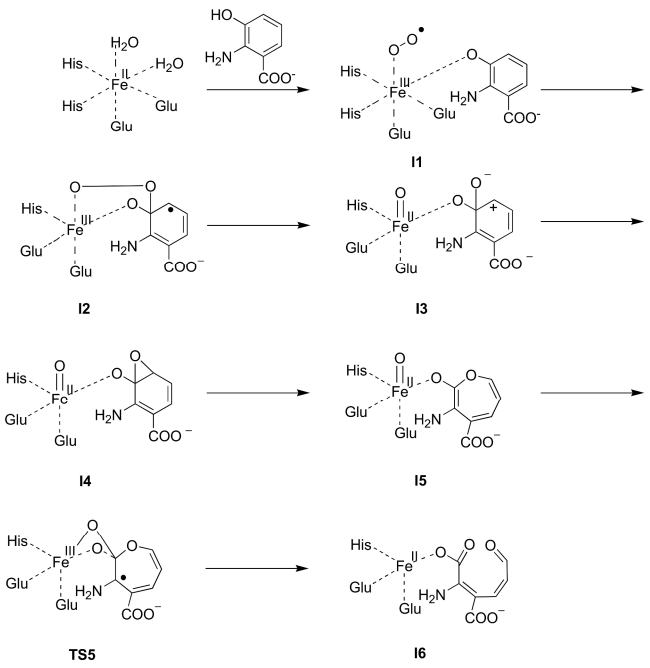

Figure 7. The reaction scheme obtained by QM and QM/MM calculations.

Details of the reaction. A notable feature of the proposed mechanism is the formation of Fe^{3+} – 3-Ohaa intermediate (I1), while *Bittner et al.*[40] has proposed the formation of the superoxo – Fe^{2+} – (iminobenzo) – semiquinonate intermediate after O_2 binding to the enzyme – substrate complex. However, the QM/MM calculations clearly indicated Fe^{2+} to Fe^{3+} transition upon oxygen binding (see Figure 7 and Supplemental Table S4b) in the presence of the substrate stabilized by the

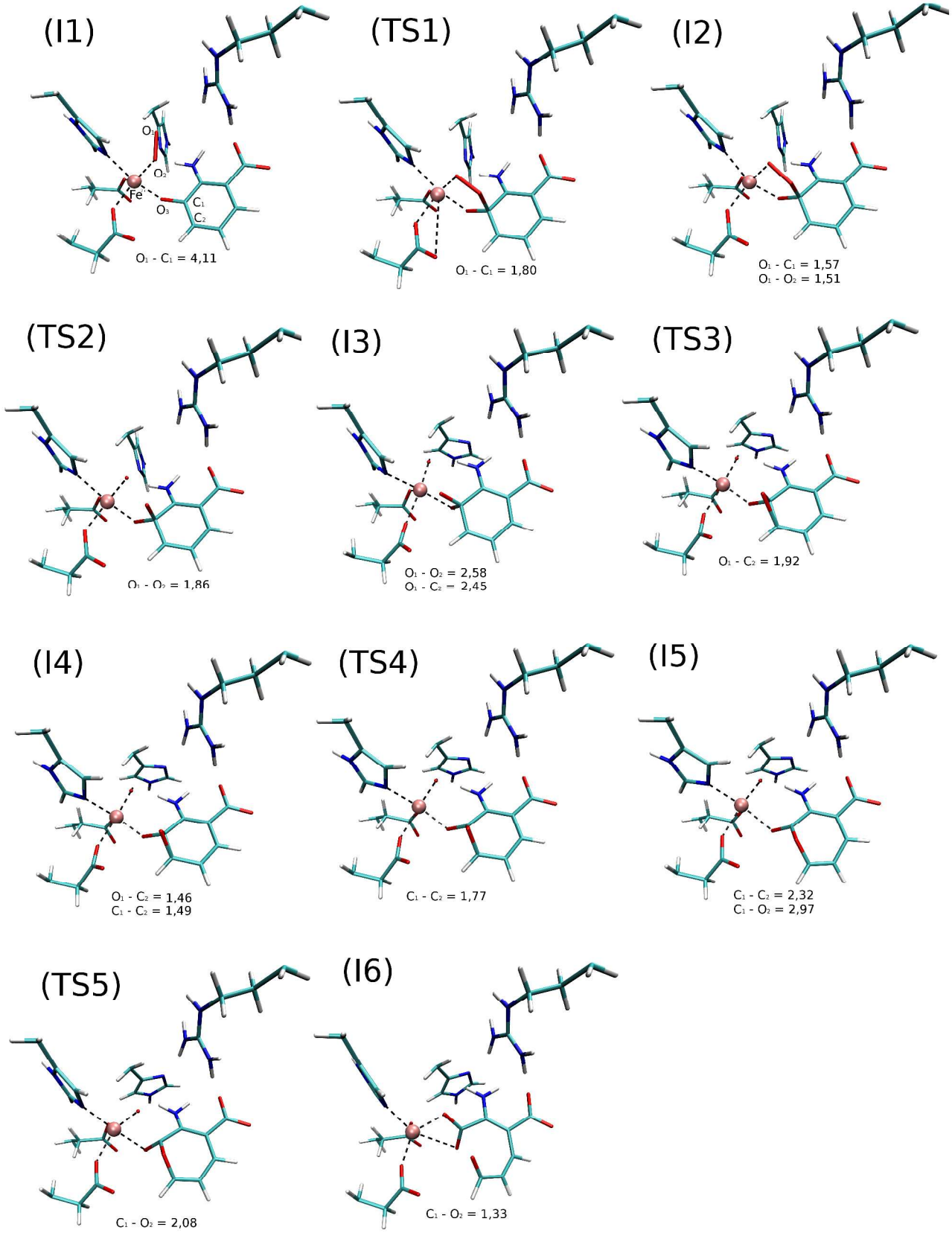

Figure 8. The full reaction mechanism obtained by the QM/MM (ONIOM) approach using mechanical embedding calculations. The stationary points (TS and minima) are shown. The distances between the reacting atoms are given in Å.

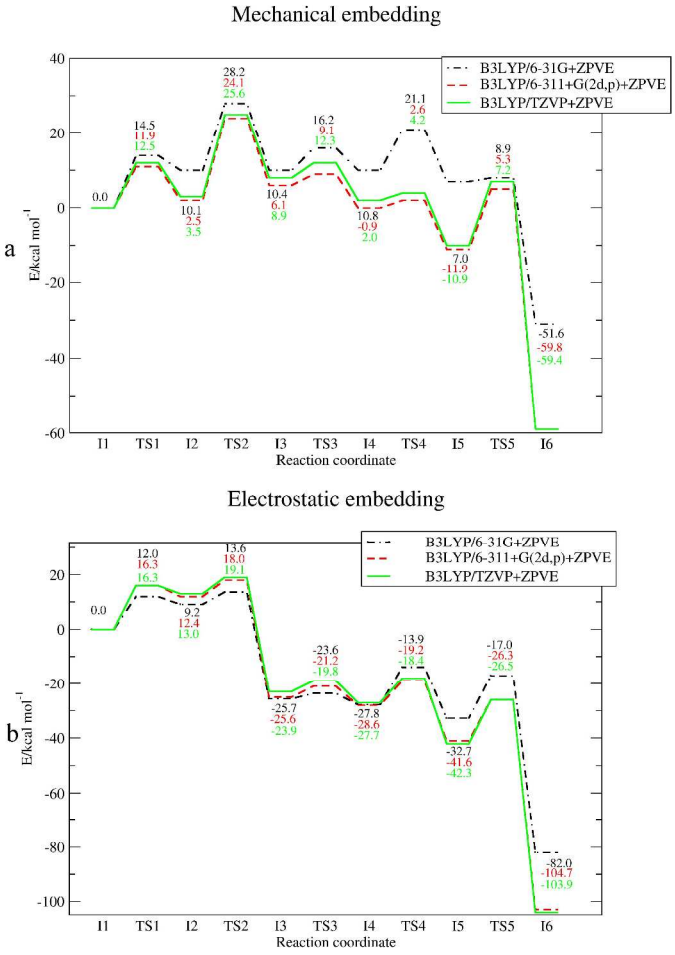

Figure 9. The energy profile for the reaction mechanism obtained by QM/MM (B3LYP/6-31G:AMBER(ff96)) calculations (black dash line with dots) and corrected using the higher basis sets, 6-311+G(2d,p) (red dashed line), and TZVP (green line): a) using mechanical embedding calculations; b) using electronic embedding.

Arg43 side chain. There are also some disparities in our reaction mechanism compared to the proposed one. We found the existence of metastable zwitterionic intermediate I3 that was not present in the mechanism of *Znag et al.*[10]. Further, the epoxy intermediate I4 is not a radical species in our mechanism. Instead, we observed a reduction of Fe^{3+} to Fe^{2+}. It should be noted that in in the active site of 3HAO, 3-Ohaa coordinates Fe^{3+} monodentately (Figure 8). This is different from the 3HAO catalysed reaction proposed by *Znag et al.*[10] (Figure 1) and the synthetic model of 3HAO[40], as well as from the reaction determined for homoprotocatechuate 2,3-dioxygenase (2,3-HPCD) by *Mbughuni et al.*[41]. In the reaction proposed by *Zhang et al.* the substrate, 3-Ohaa coordinates Fe^{3+} bidentately by O^- (deprotonated hydroxyl) and NH^- (deprotonated amino group). Similarly, in the active site of 2,3-HPCD, 4-nitrocatechol coordinates Fe^{3+} bidentately by two O^- (deprotonated hydroxyls). On the other hand, in the crystal structure of the rigid synthetic model of 3HAO where tris(pyrazolyl) borate (^{Ph2}Tp) mimic the His_2Glu coordination environment, the substrate, 2-amino-4,6-di-*tert*-butylphenol anion coordinates Fe^{2+} by O^- and NH_2.

Moving the superoxo oxygen, O1, to the substrate C1 (initial and final distances are 4.11 and 1.57 Å, respectively), the first transition state of the 3HAO catalysed reaction mechanism (TS1, see Figure 8) was located with the relative energy of 11.9 kcal/mol (6-311+G(2d,p)), see Figure 9. At the point where the first reaction coordinate O1 – C1, i. e. the oxygen molecule and substrate distance reduced from 4.11 Å (initial value) to 1.57 Å at the second stationary point I2 (the relative energy 2.5 kcal/mol) was determined. In the second step the O1–O2 bond was cleaved with the reaction barrier of 21.6 kcal/mol and the related intermediate, I3 with energy of 6.1 kcal mol^{-1} above the energy of the initial state was determined as the least stable minimum at the reaction profile obtained using mechanical embedding (Figure 9a). In the next step O1 binds to C2, the neighbour C atom of the substrate phenyl ring (initial and final distances are 2.45 and 1.46 Å, respectively) with the energy barrier of 3.0 kcal mol^{-1} and in corresponding minimum (I4) oxygen is bonded with both neighbour carbon atoms. The transition state of oxygen incorporation into the ring (TS4) has a barrier of 3.5 kcal mol^{-1}, and in in following minima (I5) a seven membered ring is formed. In the last step the second oxygen molecule atom, O2, binds to the substrate C1 atom (initial and final O–C1 distances are 2.77 and 1.33 Å, respectively). The barrier for this reaction is 17.2 kcal mol^{-1}, and the energy of the product is 59.8 kcal mol^{-1} lower than the reactant (I1) energy. Inclusion of electrostatic influence of the protein environment, electronic embedding, into the QM calculations lowered the barriers of transition states according to the preceding minima, which implies that the reaction is carried out even faster than proposed with ME results (Figure 9). The nature of the stationary points was proven by frequency analysis: the reactants, products and intermediates (Is, Figure 8) do not have an imaginary frequency, while each transition state has exactly one imaginary frequency.

Discussion. Using MD simulations we studied the influence of both, the ligand binding, and the point mutations (Arg43Ala, Arg95Ala and Glu105Ala) on the structure and dynamics of the human 3HAO. It was found that the hexacoordinated iron, in the ligand free enzyme, becomes pentacoordinated in the complexes with 3-Ohaa. We could conclude that during the enzymatic reaction the vacant position, in the first coordination sphere of the metal, is occupied by an oxygen molecule in the complex. In the glutamate mutant complex with 3-Ohaa, differently than in the other variants, the substantial population of the hexacoordinated metal ion was determined during the MD simulations, so, we assume that the oxygen binding is hindered in this mutant. In line with this is the reduced enzymatic activity of the Glu105Ala mutant.

Our study showed that, besides taking role in the stabilization of the transition state (as determined by QM/MM calculations), Arg43 and Arg95 ensure the proper polarity for the iron ion. Their mutation to alanine eases metal ion oxidation in the ligand free protein (the Fe^{2+} to Fe^{3+} transition in the presence of atmospheric oxygen) and, as a consequence, its inactivation. Namely, the unfavourable Fe^{2+} to Fe^{3+} transition in the ligand free enzyme could easier occur in the Arg mutants than in the wild type protein, and consequently reduce the catalytic potency of these mutants. The other interesting finding is presence of Glu49 in the Fe^{2+} coordination sphere in the case when the substrate is bound.

To summarize, on the basis of the structural changes traced during the MD simulations, we suggested possible reasons for the reduced enzymatic activities of the 3HAO mutants. In the glutamate mutant the reduced enzymatic activity is probably caused by the lower potency of Fe^{2+} to bind oxygen molecule, while in the Arg mutants possible reasons for lower enzymatic activity are the poor stabilization of the transition state and the

reduced ability of the metal ion to activate the oxygen molecule.

Finally, we also modelled the 3HAO catalysed oxidative transformation of 3-hydroxyanthranilic acid to 2-amino-3-carboxymuconic acid semialdehyde using QM/MM approach. We found that the reaction take place over five intermediates separated by the five first order transition states (see Figures 8 and 9). The reaction is very exergonic with the final energy of the system 59.8 kcal mol^{-1} lower than the initial and the highest energy barriers surmounted by the system are related to the oxygen transfer (TS1 and TS5). The resulting product is coordinated to Fe^{2+} monodentately, *via* carboxyl group, while the other carboxyl group is, similarly to the initial state, hydrogen bonded to Arg43.

Conclusions

An exhaustive multilevel computational study enabled us to determine the reaction mechanism of the 3HAO catalysed oxidative degradation of 3-Ohaa. It was found that upon the substrate, 3-Ohaa, binding the metal coordination number reduces from six to five, in accord with the proposed enzymatic reaction. In the 3HAO – 3-Ohaa complex, the vacant position in the first coordination sphere of Fe^{2+} is occupied by an oxygen molecule resulting with the metal ion, $Fe^{2+} \rightarrow Fe^{3+}$, reduction. The QM/MM study showed that the reaction is very exergonic and that the highest energy barriers in the reaction profile are related to the oxygen transfer. Influence of the point mutations Arg43Ala, Arg95Ala and Glu105Ala on the protein structure and dynamics was determined. The results enabled us to rationalize the experimentally determined significantly lower enzymatic activity of these mutants.

Acknowledgements

The authors acknowledge the Ministry of Science, Education, and Sport of the Republic of Croatia (project 098-1191344-2860) for the financial support. The calculations were performed using the Isabella computing cluster (www.srce.unizg.hr/en/isabella/) and the Croatian national GRID infrastructure (www.cro-ngi.hr).

Notes and references

[a] Faculty of Medicine, J. Huttlera 4, HR-31000 Osijek, Croatia.

[b] Ruđer Bošković Institute, Bijenička 54, HR-10000 Zagreb, Croatia.

Electronic Supplementary Information (ESI) available: [filename: suppl_brkic_kovacevic_tomic.docx]. See DOI: 10.1039/b000000x/

1. http://www.uniprot.org/uniprot/P46952.
2. P. Malherbe, C. Köhler, M. Da Prada, G. Lang, V. Kiefer, R. Schwarcz, H.-W. Lahm and A. M. Cesura, *Journal of Biological Chemistry*, 1994, **269**, 13792-13797.
3. A. C. Foster, R. J. White and R. Schwarcz, *J Neurochem*, 1986, **47**, 23-30.
4. R. Schwarcz, C. A. Tamminga, R. Kurlan and I. Shoulson, *Annals of neurology*, 1988, **24**, 580-582.
5. F. Du, J. Williamson, E. Bertram, E. Lothman, E. Okuno and R. Schwarcz, *Neuroscience*, 1993, **55**, 975-989.
6. D. Zadori, P. Klivenyi, E. Vamos, F. Fülöp, J. Toldi and L. Vecsei, *Journal of neural transmission*, 2009, **116**, 1403-1409.
7. E. Bitto, C. A. Bingman, G. E. Wesenberg and G. N. Phillips Jr., *in preparation*, 2007.
8. S. Fetzner, *Applied and environmental microbiology*, 2012, **78**, 2505-2514.
9. K. L. Colabroy, H. Zhai, T. Li, Y. Ge, Y. Zhang, A. Liu, S. E. Ealick, F. W. McLafferty and T. P. Begley, *Biochemistry*, 2005, **44**, 7623-7631.
10. Y. Zhang, K. L. Colabroy, T. P. Begley and S. E. Ealick, *Biochemistry*, 2005, **44**, 7632-7643.
11. D. Case, T. Darden, T. Cheatham III, C. Simmerling, J. Wang, R. Duke, R. Luo, R. Walker, W. Zhang and K. Merz, *AMBER 12*, (2012), San Francisco.
12. W. Humphrey, A. Dalke and K. Schulten, *Journal of molecular graphics*, 1996, **14**, 33-38.
13. J. Wang, W. Wang, P. A. Kollman and D. A. Case, *Journal of molecular graphics and modelling*, 2006, **25**, 247-260.
14. W. D. Cornell, P. Cieplak, C. I. Bayly, I. R. Gould, K. M. Merz, D. M. Ferguson, D. C. Spellmeyer, T. Fox, J. W. Caldwell and P. A. Kollman, *Journal of the American Chemical Society*, 1995, **117**, 5179-5197.
15. H. Brkić, D. Buongiorno, M. Ramek, G. Straganz and S. Tomić, *JBIC Journal of Biological Inorganic Chemistry*, 2012, **17**, 801-815.
16. L. A. Curtiss, M. P. McGrath, J. P. Blaudeau, N. E. Davis, R. C. Binning Jr and L. Radom, *The Journal of chemical physics*, 1995, **103**, 6104-6113.
17. M. Frisch, G. Trucks, H. B. Schlegel, G. Scuseria, M. Robb, J. Cheeseman, G. Scalmani, V. Barone, B. Mennucci and G. Petersson, *Gaussian 09, Revision A. 02, Gaussian*, (2009), Inc., Wallingford, CT.
18. V. Barone and M. Cossi, *The Journal of Physical Chemistry A*, 1998, **102**, 1995-2001.
19. M. Glušič, J. Stare, J. Grdadolnik and R. Vianello, *Journal of inorganic biochemistry*, 2013, **119**, 90-94.
20. T. A. Tatusova and T. L. Madden, *FEMS microbiology letters*, 1999, **174**, 247-250.
21. O. Trott and A. J. Olson, *Journal of computational chemistry*, 2010, **31**, 455-461.
22. W. L. Jorgensen, J. Chandrasekhar, J. D. Madura, R. W. Impey and M. L. Klein, *The Journal of chemical physics*, 1983, **79**, 926-935.
23. T. Darden, D. Pearlman and L. G. Pedersen, *The Journal of chemical physics*, 1998, **109**, 10921-10935.
24. T. Darden, D. York and L. Pedersen, *The Journal of chemical physics*, 1993, **98**, 10089-10092.
25. A. W. Götz, M. J. Williamson, D. Xu, D. Poole, S. Le Grand and R. C. Walker, *Journal of chemical theory and computation*, 2012, **8**, 1542-1555.
26. R. Salomon-Ferrer, A. W. Götz, D. Poole, S. Le Grand and R. C. Walker, *Journal of Chemical Theory and Computation*, 2013, **9**, 3878-3888.
27. T. Schneider and E. Stoll, *Physical Review B*, 1978, **17**, 1302.
28. H. J. Berendsen, J. P. M. Postma, W. F. van Gunsteren, A. DiNola and J. Haak, *The Journal of chemical physics*, 1984, **81**, 3684-3690.
29. J.-P. Ryckaert, G. Ciccotti and H. J. Berendsen, *Journal of Computational Physics*, 1977, **23**, 327-341.
30. J. M. Swanson, R. H. Henchman and J. A. McCammon, *Biophysical journal*, 2004, **86**, 67-74.
31. M. L. Connolly, *Journal of Applied Crystallography*, 1983, **16**, 548-558.
32. S.-L. Chen, W.-H. Fang and F. Himo, *The Journal of Physical Chemistry B*, 2007, **111**, 1253-1255.
33. T. Dunning Jr, P. Hay and H. Schaefer III, *Modern Theoretical Chemistry*, Plenum Press, New York, 1976.
34. P. Tao, J. F. Fisher, Q. Shi, T. Vreven, S. Mobashery and H. B. Schlegel, *Biochemistry*, 2009, **48**, 9839-9847.
35. A. Schäfer, C. Huber and R. Ahlrichs, *The Journal of Chemical Physics*, 1994, **100**, 5829-5835.
36. A. Schäfer, H. Horn and R. Ahlrichs, *The Journal of Chemical Physics*, 1992, **97**, 2571-2577.
37. T. Vreven, K. S. Byun, I. Komáromi, S. Dapprich, J. A. Montgomery, K. Morokuma and M. J. Frisch, *Journal of Chemical Theory and Computation*, 2006, **2**, 815-826.
38. G. Dong, S. Shaik and W. Lai, *Chemical Science*, 2013, **4**, 3624-3635.
39. H. Park, J. S. Baus, S. V. Lindeman and A. T. Fiedler, *Inorganic chemistry*, 2011, **50**, 11978-11989.
40. M. M. Bittner, S. V. Lindeman and A. T. Fiedler, *Journal of the American Chemical Society*, 2012, **134**, 5460-5463.
41. M. M. Mbughuni, M. Chakrabarti, J. A. Hayden, E. L. Bominaar, M. P. Hendrich, E. Münck and J. D. Lipscomb, *Proceedings of the National Academy of Sciences*, 2010, **107**, 16788-16793.